Graphene Liquid Cell Electron Microscopy of Initial Lithiation in Co$_3$O$_4$ Nanoparticles

Joon Ha Chang,[†,§] Jun Young Cheong,[†,§] Sung Joo Kim,[†,∥] Yoon-Su Shim,[†] Jae Yeol Park,[†] Hyeon Kook Seo,[†,⊥] Kyun Seong Dae,[†] Chan-Woo Lee,[‡] Il-Doo Kim,[*,†] and Jong Min Yuk[*,†]

[†]Department of Materials Science and Engineering, Korea Advanced Institute of Science and Technology, 335 Science Road, Daejeon 34141, Republic of Korea

[‡]Platform Technology Laboratory, Korea Institute of Energy Research, 152 Gajeong-Ro, Yuseong-Gu, Daejeon 34129, Republic of Korea

S Supporting Information

ABSTRACT: As it governs the overall performance of lithium-ion batteries, understanding the reaction pathway of lithiation is highly desired. For Co$_3$O$_4$ nanoparticles as anode material, here, we report an initial conversion reaction pathway during lithiation. Using graphene liquid cell electron microscopy (GLC-EM), we reveal a CoO phase of the initial conversion product as well as morphological dynamics during Co$_3$O$_4$ lithiation. In accordance with the in situ TEM observation, we confirmed that the Co$_3$O$_4$ to CoO conversion is a thermodynamically favorable process by calculating the theoretical average voltage based on density functional theory. Our observation will provide a useful insight into the oxide electrode that undergoes conversion reaction.
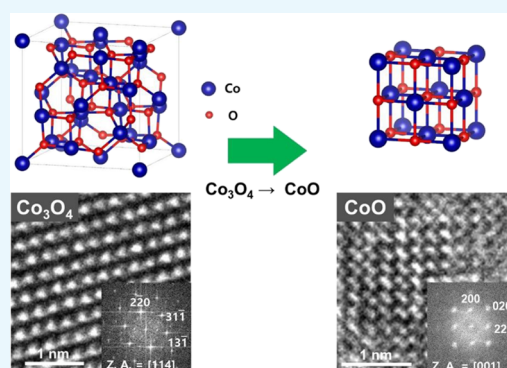
1. INTRODUCTION

Whereas lithium (Li)-ion batteries have been widely used in various applications such as laptops, electric vehicles, and so forth,[1−3] high-capacity anode materials are desired for light and portable devices.[4,5] Cobalt (II,III) oxide (Co$_3$O$_4$) is one of the promising materials because of its superior theoretical capacity (1100 mA h g^{-1}).[6−11] It is known that the Co$_3$O$_4$ anode has severe volume aggregation at high C-rates[12] and undergoes either of two different lithiation pathways.[13] One pathway involves the Li-intercalation process followed by full conversion to Co and Li$_2$O

$$Co_3O_4 + xLi \rightarrow Li_xCo_3O_4$$

$$Li_xCo_3O_4 + (8 - x)Li \rightarrow 3Co + 4Li_2O$$
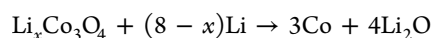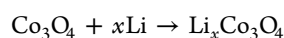
The other is the reaction pathway through the CoO phase, followed by full conversion to Co and Li$_2$O

$$Co_3O_4 + 2Li \rightarrow Li_2O + 3CoO$$

$$3CoO + Li_2O + 6Li \rightarrow 4Li_2O + 3Co$$
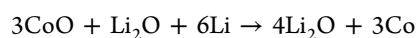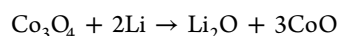
Although the pathway accompanying the Li-intercalation process has been frequently studied,[14−16] the conversion process of Co$_3$O$_4$ to CoO is still ambiguous because of a lack of direct observation.

Here, we realize the direct observation on the initial conversion of Co$_3$O$_4$ to CoO upon lithiation by using graphene liquid cell electron microscopy (GLC-EM), which has been used to acquire high-resolution imaging in a liquid electrolyte solution.[17−19] Furthermore, density functional theory (DFT) calculation is adopted to calculate the relative voltage profile, and the calculations confirm that the Co$_3$O$_4$ to CoO conversion follows a thermodynamic pathway.

2. RESULTS AND DISCUSSION

Co$_3$O$_4$ nanoparticles are prepared by ball-milling for 12 h. Figure 1a shows a bright-field transmission electron microscopy (BF−TEM) image of Co$_3$O$_4$ nanoparticles and Figure 1b shows the corresponding selected area electron diffraction (SAED) pattern. The diameters of particles are 10−40 nm, which well correspond to the calculated average crystal
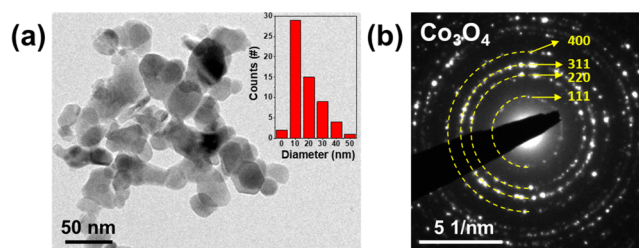

Figure 1. (a) BF−TEM image (inset: particle size distribution graph) and (b) SAED pattern of Co$_3$O$_4$ nanoparticles.
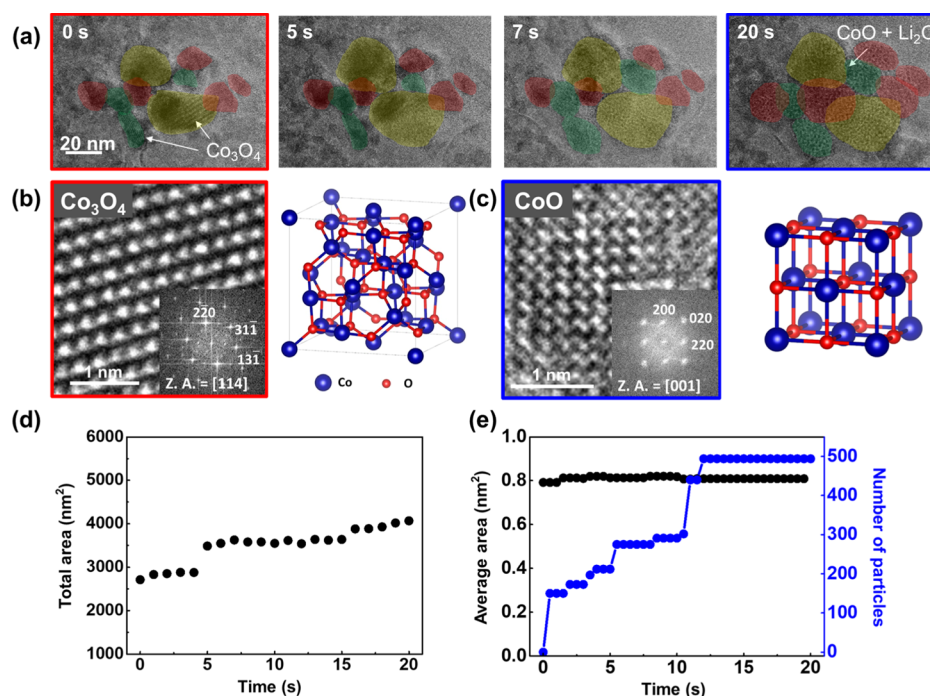
Figure 2. (a) Time-series TEM images of Co_3O_4 nanoparticles under lithiation. (b) HRTEM image and crystal structure of Co_3O_4 (before lithiation) and (c) CoO (after lithiation). (d) Total area of the particles with time. (e) Average size and number of CoO nanocrystals with time.

diameter of 24.6 nm from an X-ray diffraction (XRD) pattern (Figure S1) according to Scherrer eq 1

$$\tau = K\lambda / \beta \cos(\theta) \tag{1}$$

In order to investigate the morphological dynamics during the initial conversion reaction, in situ GLC−TEM is conducted. The GLC is prepared by encapsulating liquid electrolyte with Co_3O_4 nanoparticles between two graphene sheets. The liquid electrolyte is 1.3 M of ($LiPF_6$) dissolved in a solvent mixture consisting of 3:7 volumetric ratio of ethylene carbonate/diethyl carbonate (EC/DEC) and 10 wt % of fluoroethylene carbonate (FEC), which was used in our previous studies.[17−19] Chemical lithiation is initiated by the decomposition of $LiPF_6$ to Li by dissolution of electrons and radicals under electron beam irradiation.[17−19] The schematic diagram of the fabricated GLC is shown in Figure S2a. A high-angle annular dark-field scanning transmission electron microscopy (HAADF−STEM) image and the corresponding energy-dispersive spectroscopy (EDS) mapping of C, O, F, P, and Co are shown in Figure S2b to observe the morphology and element distribution. Co_3O_4 nanoparticles are observed inside the graphene sheets and liquid electrolyte, and all of the chemical components of the electrolyte (C, O, F, P) are shown in all parts of the HAADF−STEM image, but Co is selectively present at the place where Co_3O_4 nanoparticles locate.

Using the GLC, a direct visualization on the initial conversion reaction of Co_3O_4 to CoO is realized. The time-sequential TEM images in Figure 2a show the lithiation process of individual Co_3O_4 nanoparticles. The conversion of Co_3O_4 to CoO happens particle by particle (yellow to green to red). Ultrasmall nanocrystals are generated and embedded within the amorphous matrix and their morphology is similar to the lithiated Co_3O_4 particles in a previously reported work.[20] Figure 2b,c shows high-resolution transmission electron microscopy (HRTEM) images and corresponding crystal schematics, which confirm pre- and post-lithiated crystal

structures. During lithiation, clearly the phase transition from Co_3O_4 to CoO occurred. The total area change versus time is shown in Figure 2d. As lithiation and volume expansion happen particle by particle, volume expansion occurs step by step. The formed CoO nanocrystals and their total number is shown in Figure 2e. The number of nanocrystals also increases step by step, which has a similar trend to the total volume increase. The average size of the nanocrystals remains constant, where stable morphology and phase are maintained during TEM observation because of a small amount of liquid inside the GLC, which is not enough to fully lithiate the particles.

In addition, this crystal structure change is also identified with SAED patterns (Figure 3a,b). In accordance with HRTEM images, the phase transition from Co_3O_4 to CoO is observed in the GLC. In Figure 3c,d, electron energy loss spectroscopy (EELS) of the Co-$L_{2,3}$ edge is shown before and after lithiation. The average ratios of L_3/L_2 are measured as 2.39 and 4.51, which corresponds to the value of Co_3O_4 (1/3 Co^{2+} and 2/3 Co^{3+}) and CoO (Co^{2+}) reported in previous literature.[20,21]

To further delve into the theoretical aspects of the conversion reaction of Co_3O_4 to CoO, the average voltage V of electrode is determined using the following equation, based on Nernst eq 2

$$V = -\frac{E(\text{charge}) - E(\text{discharge}) - xE(\text{Li})}{xe} \tag{2}$$

where $E(\text{charge})$ and $E(\text{discharge})$ are the DFT energies of the charged and discharged phases, respectively. $E(\text{Li})$, x, and e are the DFT energy per atom of bulk Li, the number of the Li atoms, and elementary charge, respectively.

Here, two different reaction pathways are considered and plotted in Figure 4: (i) the conversion of Co_3O_4 into CoO and (ii) the intercalation of Li into Co_3O_4 ($LiCo_3O_4$). In the case of the first pathway, the formation of CoO takes place at 2.08 V, and Co forms subsequently at 1.81 V. On the other hand,
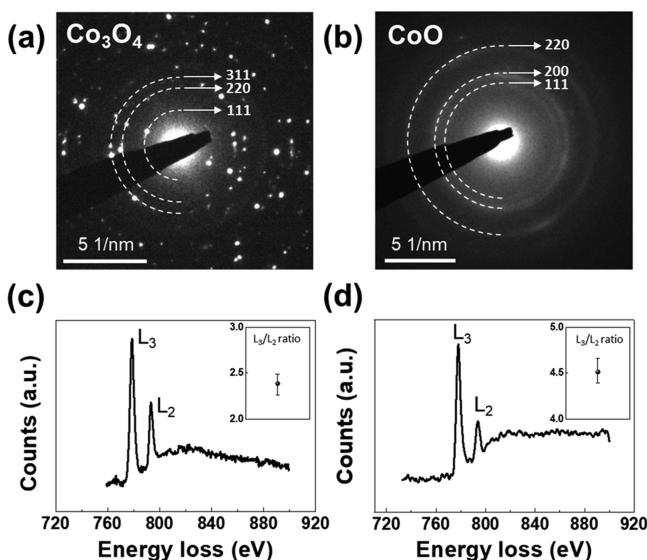
Figure 3. (a) SAED pattern before and (b) after the in situ TEM experiment. (c) EELS spectrum of the Co-L$_{2,3}$ edge before and (d) after lithiation (inset: ratio between the L$_3$ and L$_2$ peaks).
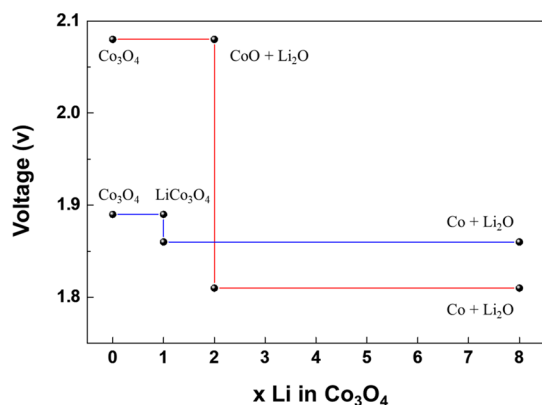

Figure 4. DFT-based voltage profile of the Li−Co$_3$O$_4$ system in the case of conversion of Co$_3$O$_4$ to CoO (red) and intercalation of Li into Co$_3$O$_4$ (LiCo$_3$O$_4$, blue).

the intercalation of Li into Co$_3$O$_4$ takes place at 1.89 V, followed by conversion to Co at 1.86 V. According to the Nernst equation, the high voltage value indicates low Gibbs-free energy changes in the reaction pathway, which corresponds to thermodynamically favorable reaction. On the basis of these results, the conversion to CoO is a favorable process with respect to Li intercalation into Co$_3$O$_4$. As lithiation in the GLC is chemical lithiation,[17−19] it follows the thermodynamic reaction pathway and transition from Co$_3$O$_4$ to CoO takes place, which corresponds with our GLC results.

To prove that the reaction in GLC−TEM actually occurs in the real electrochemical battery cell experiment, ex situ experiments are conducted. Figure S3a shows the galvanostatic charge−discharge profile of the first cycle and Figure S3b−d shows the SAED patterns at each voltage level. At 1.2 V, the phase transition of CoO is found and at the end of the discharge, both CoO and Co phases are present. Ex situ EELS is also obtained to analyze the electronic structure of lithiated Co$_3$O$_4$ (Figure S4). The positions and ratios of the L$_3$ and L$_2$ peaks well match with the EELS spectrum from the in situ experiment. Additional electrochemical information such as

cyclic voltammetry (CV), electrochemical impedance measurement, and galvanostatic charge−discharge tests for subsequent cycles are provided in the previous study.[22] The CV analysis clearly matches with the reaction pathway seen in this report, where two cathodic peaks are present at 0.75 and 0.6 V, attributed to the reduction of Co$_3$O$_4$ to CoO and subsequently CoO to Co.

3. CONCLUSIONS

In conclusion, during the initial lithiation stage, we demonstrate that Co$_3$O$_4$ nanoparticles change into CoO phases rather than intercalation phases using GLC−TEM. The DFT calculation further demonstrates that the conversion of Co$_3$O$_4$ to CoO follows a thermodynamic pathway, where chemical lithiation triggered in the GLC is a thermodynamically favorable process. As the lithiation pathway considerably affects the reaction kinetics, cycle retention characteristics, and rate capabilities,[23−25] our study will provide an insight into designing anode materials of spinel oxide with multiple oxidation states.

4. EXPERIMENTAL SECTION

4.1. Materials and Fabrication of the GLC. Co$_3$O$_4$ nanoparticles were purchased from Sigma-Aldrich. For the fabrication of the GLC, the multilayer graphene was initially synthesized. Using Cu foil (99.8%, Alfa Aesar) as the substrate, graphene was synthesized by using chemical vapor deposition (CVD). Then, the Cu foil was etched with 20% phosphoric acid (H$_3$PO$_4$, 85%, Junsei) for 20 min for removing impurities and oxides. As for the conditions of CVD, the temperature was set to 1050 °C for 30 min and stabilized for 60 min under 200 standard cubic centimeters per minute (sccm) of hydrogen (H$_2$) gas. Subsequently, 20 sccm of methane (CH$_4$) gas, which acted as the carbon source, was injected for 25 min and was later cooled to room temperature at a rapid rate. Such a synthesized multilayer graphene was transferred to a holey carbon Au TEM grid (quantifoil, 300 mesh, hole size = 2 μm). Ammonium persulfate (0.2 M, (NH$_4$)$_2$S$_2$O$_8$, Sigma-Aldrich) was used to etch the Cu foil for 6 h. Then, it was washed with water to remove the (NH$_4$)$_2$S$_2$O$_8$. The GLC was prepared by dropping 20 μL of the electrolyte mixture containing Co$_3$O$_4$ nanoparticles, lithium hexafluorophosphate (LiPF$_6$), and EC/DEC (v/v = 3:7) with 10 wt % of FEC on one graphene-transferred grid and placing another graphene-transferred grid on the top.[26] Liquid cells were formed during spontaneous drying by graphene sheets by the van der Waals force.

4.2. In Situ TEM Observation. To carry out the in situ TEM observation, a Titan ETEM G^2 microscope (FEI) was used at an operating voltage of 300 kV. The range of the electron beam dosage was between 800 and 1000 e$^-$/Å^2 s. The dynamics in the process of lithiation upon e-beam irradiation were recorded in a charge-coupled device camera (Gatan Ultrascan 1000). Furthermore, EDS elemental mapping was obtained using JEOL JEM 2100F under a 200 kV accelerating voltage. EELS analysis was conducted using GIF Quantum 966 in a Titan ETEM G^2 microscope (FEI).

4.3. Other Characterizations. The crystal structures of Co$_3$O$_4$ were confirmed by an X-ray diffractometer (XRD, D/MAX-2500, Rigaku) using Cu Kα radiation (λ = 1.54 Å). Ex situ TEM images and SAED patterns of Co$_3$O$_4$ nanoparticles were taken using JEOL JEM 2100F under a 200 kV accelerating voltage.

4.4. Particle Analysis. To measure the average size and area of the particles, the following methods were used. First, time-series images were extracted from the movie at 0.5 s intervals. Second, the edge of the CoO nanocrystals were drawn to sharpen the boundaries. Finally, using "Analyze Particles" plugins in ImageJ software, the number and area of nanocrystals were calculated.

4.5. Computational Details. DFT calculations are performed using the Vienna Ab initio Simulation Package[27] within the projector-augmented wave scheme as formulated by Perdew−Burke−Ernzerhof[28] with spin-polarization. A cutoff energy of 520 eV is adopted for the plane-wave expansion of wave functions and k-point grids of $1000/n$ are used with the Monkhorst−Pack method for $LiCo_3O_4$ and the γ-centered method for all others, where n is the number of atoms in the supercell. A Hubbard U term of 3.32 eV is chosen for Co^{2+} and Co^{3+} based on previous literature.[14,29−32] The DFT energies are converged within 1.0×10^{-6} eV. All structures in our study are based on those from the Materials Project[33] which are fully relaxed using the aforementioned settings.

4.6. Ex Situ Electrochemical Test. The electrochemical cell testing was conducted in a manner similar to the previously reported literature.[22] Briefly, the electrochemical cells were fabricated in the Ar-filled glove box, with a 2032-type coin cell. To start with, the slurry was made in a mortar, with Co_3O_4 nanoparticles, binder, and carbon black, in a weight ratio of 8:1:1. The binder consisted of carboxymethyl cellulose and polyacrylic acid, in a weight ratio of 1:1. The slurry was casted onto the Cu foil, dried at 60 °C for 10 min, and dried inside the vacuum oven at 150 °C for 2 h to completely remove the solvent. The average amount of loaded active materials was 1.5 mg cm^{-2}. The electrochemical cell was assembled with a counter electrode (Li foil), a separator (Celgard 2325), a slurry-casted electrode, a spacer, a spring, and an electrolyte. The electrolyte consisted of 1.3 M lithium hexafluorophosphate ($LiPF_6$) in organic solvent of EC/DEC with 10 wt % of FEC. The CV was conducted with a scan rate of 0.1 mV s^{-1} in the voltage range of 0.01−3.0 V. After the specific electrochemical cell test, the electrochemical cells were transferred to the antechamber of the glove box, the cells were disassembled, and the electrode was washed with dimethyl carbonate prior to analysis.

ASSOCIATED CONTENT

ⓈSupporting Information

The Supporting Information is available free of charge on the ACS Publications website at DOI: 10.1021/acsomega.9b00185.

> XRD pattern of pristine Co_3O_4 nanoparticles; schematic diagram and EDS mapping of the GLC; galvanostatic charge−discharge profile and corresponding SAED patterns of the 1st cycle; ex situ EELS spectrum of Co (PDF)
>
> Real-time TEM movie showing the lithiation of Co_3O_4 nanoparticles in the GLC (MP4)

AUTHOR INFORMATION

Corresponding Authors
*E-mail: idkim@kaist.ac.kr (I.-D.K.).
*E-mail: jongmin.yuk@kaist.ac.kr (J.M.Y.).

ORCID ⊚

Joon Ha Chang: 0000-0001-8877-9917

Sung Joo Kim: 0000-0001-9776-1532
Il-Doo Kim: 0000-0002-9970-2218
Jong Min Yuk: 0000-0002-4677-7363

Present Addresses
‖S.J.K. is currently with the Department of Materials science and Engineering, Seoul National University, Seoul 08826, Republic of Korea.
⊥H.K.S. is currently with the Memory Analysis Science and Engineering group, Samsung Electronics, Hwaseong 18488, Republic of Korea.

Author Contributions
§J.H.C. and J.Y.C. contributed equally to this work.

Notes
The authors declare no competing financial interest.

REFERENCES

(1) Tarascon, J.-M.; Armand, M. Issues and Challenges Facing Rechargeable Lithium Batteries. *Nature* **2001**, *414*, 359−367.

(2) Megahed, S.; Scrosati, B. Lithium-Ion Rechargeable Batteries. *J. Power Sources* **1994**, *51*, 79−104.

(3) Scrosati, B.; Garche, J. Lithium Batteries: Status, Prospects and Future. *J. Power Sources* **2010**, *195*, 2419−2430.

(4) Xue, X.-Y.; Yuan, S.; Xing, L.-L.; Chen, Z.-H.; He, B.; Chen, Y.-J. Porous Co_3O_4 Nanoneedle Arrays Growing Directly on Copper Foils and Their Ultrafast Charging/Discharging as Lithium-Ion Battery Anodes. *Chem. Commun.* **2011**, *47*, 4718−4720.

(5) Bruce, P. G.; Freunberger, S. A.; Hardwick, L. J.; Tarascon, J.-M. $Li−O_2$ and Li−S Batteries with High Energy Storage. *Nat. Mater.* **2011**, *11*, 19.

(6) Sultana, I.; Rahman, M. M.; Ramireddy, T.; Sharma, N.; Poddar, D.; Khalid, A.; Zhang, H.; Chen, Y.; Glushenkov, A. M. Understanding Structure−Function Relationship in Hybrid $Co_3O_4−Fe_2O_3$/ C Lithium-Ion Battery Electrodes. *ACS Appl. Mater. Interfaces* **2015**, *7*, 20736−20744.

(7) Li, H.-H.; Li, Z.-Y.; Wu, X.-L.; Zhang, L.-L.; Fan, C.-Y.; Wang, H.-F.; Li, X.-Y.; Wang, K.; Sun, H.-Z.; Zhang, J.-P. Shale-like Co_3O_4 for High Performance Lithium/Sodium Ion Batteries. *J. Mater. Chem. A* **2016**, *4*, 8242−8248.

(8) Chen, S.; Zhao, Y.; Sun, B.; Ao, Z.; Xie, X.; Wei, Y.; Wang, G. Microwave-Assisted Synthesis of Mesoporous Co_3O_4 Nanoflakes for Applications in Lithium Ion Batteries and Oxygen Evolution Reactions. *ACS Appl. Mater. Interfaces* **2015**, *7*, 3306−3313.

(9) Li, Y.; Tan, B.; Wu, Y. Mesoporous Co_3O_4 Nanowire Arrays for Lithium Ion Batteries with High Capacity and Rate Capability. *Nano Lett.* **2008**, *8*, 265−270.

(10) Wang, H.; Mao, N.; Shi, J.; Wang, Q.; Yu, W.; Wang, X. Cobalt Oxide-Carbon Nanosheet Nanoarchitecture as an Anode for High-Performance Lithium-Ion Battery. *ACS Appl. Mater. Interfaces* **2015**, *7*, 2882−2890.

(11) Wu, Y.; Meng, J.; Li, Q.; Niu, C.; Wang, X.; Yang, W.; Li, W.; Mai, L. Interface-modulated fabrication of hierarchical yolk−shell Co_3O_4/C dodecahedrons as stable anodes for lithium and sodium storage. *Nano Res.* **2017**, *10*, 2364−2376.

(12) Cheng, X.; Li, Y.; Shi, H.; Lu, J.; Zhang, Y. Rate-dependent electrochemical reaction mechanism of spinel metal oxide anode studied by in situ TEM. *J. Alloys Compd.* **2018**, *763*, 349−354.

(13) Larcher, D.; Sudant, G.; Leriche, J.-B.; Chabre, Y.; Tarascon, J.-M. The Electrochemical Reduction of Co_3O_4 in a Lithium Cell. *J. Electrochem. Soc.* **2002**, *149*, A234.

(14) Li, Q.; Wu, J.; Yao, Z.; Xu, Y.; Thackeray, M. M.; Wolverton, C.; Dravid, V. P. Dynamic Imaging of Metastable Reaction Pathways in Lithiated Cobalt Oxide Electrodes. *Nano Energy* **2018**, *44*, 15−22.

(15) Li, J.; He, K.; Meng, Q.; Li, X.; Zhu, Y.; Hwang, S.; Sun, K.; Gan, H.; Zhu, Y.; Mo, Y.; et al. Kinetic Phase Evolution of Spinel Cobalt Oxide During Lithiation. *ACS Nano* **2016**, *10*, 9577−9585.

(16) Luo, L.; Wu, J.; Xu, J.; Dravid, V. P. Atomic Resolution Study of Reversible Conversion Reaction in Metal Oxide Electrodes for Lithium-Ion Battery. *ACS Nano* **2014**, *8*, 11560−11566.

(17) Cheong, J. Y.; Chang, J. H.; Seo, H. K.; Yuk, J. M.; Shin, J. W.; Lee, J. Y.; Kim, I.-D. Growth Dynamics of Solid Electrolyte Interphase Layer on SnO_2 Nanotubes Realized by Graphene Liquid Cell Electron Microscopy. *Nano Energy* **2016**, *25*, 154−160.

(18) Chang, J. H.; Cheong, J. Y.; Yuk, J. M.; Kim, C.; Kim, S. J.; Seo, H. K.; Kim, I.-D.; Lee, J. Y. Direct Realization of Complete Conversion and Agglomeration Dynamics of SnO_2 nanoparticles in Liquid Electrolyte. *ACS Omega* **2017**, *2*, 6329−6336.

(19) Cheong, J. Y.; Chang, J. H.; Kim, S. J.; Kim, C.; Seo, H. K.; Shin, J. W.; Yuk, J. M.; Lee, J. Y.; Kim, I.-D. In Situ High-Resolution Transmission Electron Microscopy (TEM) Observation of Sn Nanoparticles on SnO_2 Nanotubes Under Lithiation. *Microsc. Microanal.* **2017**, *23*, 1107−1115.

(20) Su, Q.; Zhang, J.; Wu, Y.; Du, G. Revealing the Electrochemical Conversion Mechanism of Porous Co_3O_4 Nanoplates in Lithium Ion Battery by in Situ Transmission Electron Microscopy. *Nano Energy* **2014**, *9*, 264−272.

(21) Zhao, Y.; Feltes, T. E.; Regalbuto, J. R.; Meyer, R. J.; Klie, R. F. In Situ Electron Energy Loss Spectroscopy Study of Metallic Co and Co Oxides. *J. Appl. Phys.* **2010**, *108*, 063704.

(22) Cheong, J. Y.; Chang, J. H.; Cho, S.-H.; Jung, J.-W.; Kim, C.; Dae, K. S.; Yuk, J. M.; Kim, I.-D. High-rate formation cycle of Co_3O_4 nanoparticles for superior electrochemical performance in lithium-ion batteries. *Electrochim. Acta* **2019**, *295*, 7−13.

(23) Shang, T.; Wen, Y.; Xiao, D.; Gu, L.; Hu, Y.-S.; Li, H. Atomic-Scale Monitoring of Electrode Materials in Lithium-Ion Batteries Using In Situ Transmission Electron Microscopy. *Adv. Energy Mater.* **2017**, *7*, 1700709.

(24) Huang, Q.; Yang, Z.; Mao, J. Mechanisms of the Decrease in Low-Temperature Electrochemical Performance of $Li_4Ti_5O_{12}$-Based Anode Materials. *Sci. Rep.* **2017**, *7*, 15292.

(25) Kim, S. J.; Chang, D.; Zhang, K.; Graham, G.; Van der Ven, A.; Pan, X. Accordion Strain Accommodation Mechanism within the Epitaxially Constrained Electrode. *ACS Energy Lett.* **2018**, *3*, 1848−1853.

(26) Chang, J. H.; Cheong, J. Y.; Seo, H. K.; Kim, I.-D.; Yuk, J. M. Preparation of Graphene Liquid Cells for the Observation of Lithium-ion Battery Material. *J. Vis. Exp.* **2019**, No. e58676.

(27) Kresse, G.; Furthmüller, J. Efficient iterative schemes for ab initio total-energy calculations using a plane-wave basis set. *Phys. Rev. B: Condens. Matter Mater. Phys.* **1996**, *54*, 11169.

(28) Perdew, J. P.; Burke, K.; Ernzerhof, M. Generalized Gradient Approximation Made Simple. *Phys. Rev. Lett.* **1996**, *77*, 3865−3868.

(29) Wang, L.; Maxisch, T.; Ceder, G. Oxidation energies of transition metal oxides within the GGA+U framework. *Phys. Rev. B: Condens. Matter Mater. Phys.* **2006**, *73*, 195107.

(30) Montoya, A.; Haynes, B. S. Periodic density functional study of Co_3O_4 surfaces. *Chem. Phys. Lett.* **2011**, *502*, 63−68.

(31) Jain, A.; Hautier, G.; Ong, S. P.; Moore, C. J.; Fischer, C. C.; Persson, K. A.; Ceder, G. Formation enthalpies by mixing GGA and GGA + U calculations. *Phys. Rev. B: Condens. Matter Mater. Phys.* **2011**, *84*, 045115.

(32) Yu, X.-Y.; Meng, Q.-Q.; Luo, T.; Jia, Y.; Sun, B.; Li, Q.-X.; Liu, J.-H.; Huang, X.-J. Facet-dependent electrochemical properties of Co_3O_4 nanocrystals toward heavy metal ions. *Sci. Rep.* **2013**, *3*, 2886.

(33) Jain, A.; Ong, S. P.; Hautier, G.; Chen, W.; Richards, W. D.; Dacek, S.; Cholia, S.; Gunter, D.; Skinner, D.; Ceder, G.; Persson, K. A. Commentary: The Materials Project: A materials genome approach to accelerating materials innovation. *APL Mater.* **2013**, *1*, 011002.